Experimental Demonstration of a Terahertz Frequency Reference based on Coherent Population Trapping

Mathieu Collombon, Cyril Chatou, Gaétan Hagel, Jofre Pedregosa-Gutierrez, Marie Houssin, M. Knoop, Caroline Champenois

Experimental Demonstration of a Terahertz Frequency Reference based on Coherent Population Trapping

M. Collombon, C. Chatou, G. Hagel, J. Pedregosa-Gutierrez, M. Houssin, M. Knoop, and C. Champenois*
Aix Marseille Univ, CNRS, PIIM, Marseille, France
(Dated: March 12, 2019)

A novel protocol of interrogation based on coherent population trapping in an N-level scheme atomic system leads to dark resonances involving three different photons. An ensemble of several hundreds of radiofrequency-trapped ions is probed by three lasers simultaneously locked onto the same optical frequency comb, resulting in high-contrast spectral lines referenced to an atomic transition in the THz domain. We discuss the cause of uncertainties and limitations for this method and show that reaching a sub-kHz resolution is experimentally accessible via this interrogation protocole.

PACS numbers:

The THz science and technology has developed rapidly over the last 30 years, initially boosted by the development of laser-based THz time-domain spectroscopy. It is now expanding its development toward cw sources and detectors, such as THz quantum cascade lasers [1, 2] which offer tunable sources that allow for high resolution spectroscopy [3–5]. Among all the issues raised by the maturation of THz technologies, we are concerned here by the stringent need for THz frequency standards, as pointed out by T. Yasui in his 2013 review focused on THz frequency metrology[6].

Concerning frequency metrology, the gap between optical and electrical regions is now successfully bridged thanks to the invention of the optical frequency comb (OFC) [7], a mode-locked periodic pulsed radiation where each frequency lies in the optical domain and is separated from the next eigen-mode by a frequency interval which lies in the electrical domain. Since the invention of the OFC, the THz gap has been filled to take advantage of the coherent frequency link between the microwave, the optical and the THz regions[6, 8]. The THz range is the domain of the rotational transitions in light molecules, with natural line-widths as narrow as a few hertz which is of high relevance for detection in an astrophysics and atmospheric context as 98% of the photons released since the Big Bang are now observable in the 0.6-8 THz range [9]. Using narrow molecular lines as frequency references implies to have tunable sources and fast and sensitive detectors [10]. The first requirement is fulfilled by the development of quantum cascade lasers (QCL) [3, 4]. The second issue often implies frequency mixing to down-convert the signal to the GHz range. Taking advantage of a narrow molecular line also implies to overcome the Doppler effect that broadens absorption or emission lines. All these drawbacks of a molecular THz frequency reference can be avoided by using laser-cooled atoms as a basis and visible laser light for interrogation.

* caroline.champenois@univ-amu.fr

Following our previous theoretical work that proposed a THz frequency standard based on three-photon coherent population trapping (CPT) in stored ions [11] we report here the experimental observation of the dark line induced by this CPT in the fluorescence of a cloud of calcium ions and confirm its reference to a dipole magnetic transition at 1.8 THz. CPT builds on atomic coherence and has been demonstrated to be a very efficient tool for achieving control of the interaction between electromagnetic fields and an atomic sample. It is mostly used with two-photon processes like in CPT-clocks where the observed dark line is referenced to a hyperfine transition lying in the GHz range [12]. The three involved photons lie in the optical domain and this configuration is ideal to transmit the 1.8 THz reference signal by optical means and to benefit from very efficient detectors. Indeed, because THz radiation hardly propagates along long distances in air, its phase-coherent transfer implies to coherently duplicate its phase information onto an optical carrier[13]. Building a THz referenced signal from three coherent lasers avoids this duplication stage and allows its transmission over long distances through optical fibers.

The three-photon dark line is observed in the laser-induced fluorescence emitted by a cloud of $^{40}Ca^{+}$ ions, confined in a linear RF quadrupole trap. The calcium ions are Doppler laser-cooled on their resonance transition $4S_{1/2} \rightarrow 4P_{1/2}$ at 396.85 nm (label B). This transition is not closed and once in the excited state $4P_{1/2}$, the ions can decay to the metastable state $3D_{3/2}$ with a probability $\beta = 0.064$ [14]. Keeping the ions within the cooling cycle thus implies a second "repumping" laser, tuned on the dipole transition $3D_{3/2} \rightarrow 4P_{1/2}$ at 866.21 nm (label R). The third laser involved in the CPT process is resonant with the electric quadrupole transition $4S_{1/2} \rightarrow 3D_{5/2}$ at 729.15 nm (label C, see Fig. 1, **a** for the transition scheme).

Because it is based on a weak coupling, this last transition has a natural line-width which is 8 orders of magnitude smaller than that of the dipole transition involved in the laser cooling [15]. Despite of the weakness of the

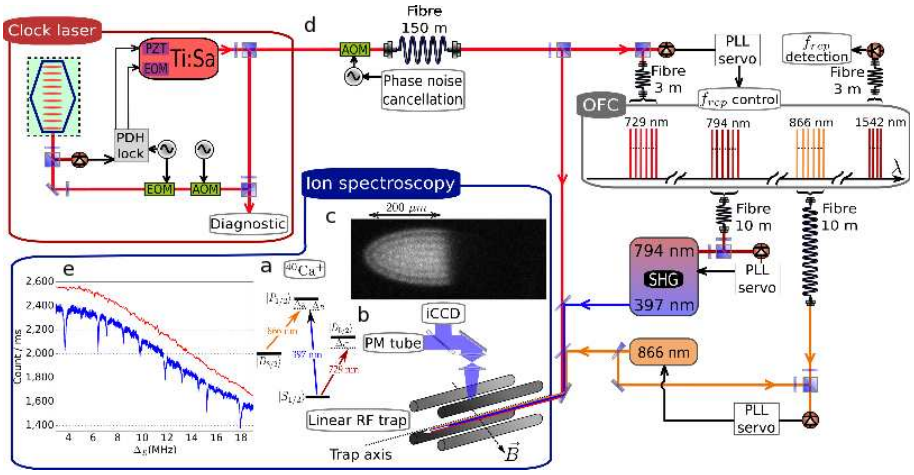

FIG. 1. **a** : Transition scheme for the 3-photon CPT in Ca^+, **b** : Schematic of the experimental set-up : the three laser beams are propagating along the trap symmetry axis, the linear radio-frequency trap is represented by its four rods, the laser induced fluorescence is recorded on a photomultiplier (PM tube) for photon counting and a intensified CCD camera for spatial resolution of the fluorescence. **c** : picture of a cloud made of 710 ($\pm$35) ions, the ions shelved in the metastable $D_{5/2}$ state or trapped in the coherent superposition are dark and split from the bright ions because they do not feel the radiation pressure induced by the cooling laser on the bright ions. **d**: set-up for the laser phase-lock, based on an OFC locked onto an ultra-stable Ti:Sa laser, **e** : Laser induced fluorescence of a cloud of laser cooled 560 ($\pm$25) ions versus the detuning of the R-laser. The top red curve shows photon counts with the cooling (B and R lasers alone ($P_B = 10$ mW, $P_R = 1$ mW) while in the lower blue curve, the 729 nm laser is added ($P_C = 12.1$ mW). Background : 570($\pm$25) counts/ms

laser-atom interaction on this transition, it can play a major role in the internal state dynamics provided that a resonance condition is fulfilled [16]. This condition can be extrapolated from two-photon Λ-scheme dark resonances [17] and it writes

$$\Delta_R = \Delta_B - \Delta_C - \delta_C \tag{1}$$

where $\Delta_R, \Delta_B, \Delta_C$ are the detuning of the three lasers and δ_C is the light-shift induced by the quadrupole coupling on the 729 nm transition [16] (see Supplemental Material for further explanation). The trapping state is a coherent superposition of the three stable and metastable dressed states that is not coupled by laser excitation and once trapped in this state, the ions do not emit any photon, provided the trapping state is stationary.

When fulfilled, the three-photon resonance condition implies a strong relation between the three laser frequencies

$$\omega_R + \omega_C - \omega_B + \delta_C = \omega_{THz} \tag{2}$$

with ω_{THz} the frequency of the magnetic dipole transition between $3D_{3/2}$ and $3D_{5/2}$, which appears as the atomic reference. The frequency ω_{THz} is 1.82 THz in Ca^+ and its absolute value is known with a $\pm$8 Hz uncertainty through Raman spectroscopy on a single trapped ion [18, 19]. Considering the typical intensity and detuning for the laser at 729 nm, δ_C ranges 1 to 100 Hz. In the following, we present the experimental conditions of observing a three-photon dark resonance in the fluorescence of a cloud of trapped ions. We review the major effects which contribute to the line-width, frequency shift and contrast of the dark line as there are the Doppler effect, the Zeeman effect and power-induced effects.

In the experiments presented here, the three lasers co-propagate along the symmetry axis of a linear quadrupole RF-trap (see Fig. 1,**b**) and the effective wave-vector $\mathbf{\Delta}\vec{k}$ is the one of the magnetic dipole transition $k_{THz} = 2\pi/\lambda_{THz}$ with λ_{THz} the $3D_{3/2}$-$3D_{5/2}$ transition wavelength, equal to 165 μm. The quadrupole trap is described in [20, 21], its main characteristics are an inner radius of 3.93 mm for a rod radius of 4.5 mm [22] and an RF trapping frequency of 5.2 MHz. For the work presented here, it is operated with an RF-voltage difference between neighbouring rods of 826 V_{pp} (Mathieu parameter $q_x = 0.24$). The Doppler-laser cooling drives the ion cloud from a gas, through the liquid, to a crystal phase [23] with a temperature estimated to be of the order of 10 mK. Once in the liquid and crystal phase, the ion cloud forms an ellipsoid [24, 25] with a diameter ranging from 80 to 280 μm and a length ranging from 120 to 740 μm for a number of ions comprised between 40 and 2750 (see Fig. 1,**c**). The 397 nm and 866 nm lasers have an elliptical section, with an aspect ratio of 2 and a mean-squared diameter at the position of the cloud equal to 4.0 mm and 4.7 mm, respectively. The laser intensity and wave-vectors can be considered as uniform all over the ion cloud. The 729 nm laser has the smallest size with a waist diameter measured to 300($\pm$20) μm. It is

still larger than the largest of the cloud diameters but its intensity is not uniform over the largest clouds. This geometric configuration does not cancel the Doppler effect which broadens the three-photon dark lines by 20 kHz (FWHM) for a sample at 10 mK, but it eliminates any broadening induced by finite interaction time, which is an identified limitation on two-photon CPT line-width when observed on an atomic beam or a gas in a cell [12, 26].

For the observation of the dark lines, the three involved lasers are admitted continuously on the cloud. They are phase-locked through a commercial offset-free optical frequency comb [27] and their frequency is measured with an uncertainty in the kHz range (see Supplemental Material and Fig. 1,**d**). A magnetic field of the order of 1 Gauss is applied and the three laser polarisations are linear, perpendicular to the trap axis and nearly perpendicular to the local magnetic field. Spectra as the one shown on figure 1,(**e**) are observed when collecting the photons emitted at 397 nm on the $4P_{1/2} \rightarrow 4S_{1/2}$ transition while the frequency of the R-laser is scanned. Typical laser powers are 10 to 20 mW at 397 nm (P_B), 0.5 to 5 mW at 866 nm (P_R) and 5 to 25 mW at 729 nm (P_C). A maximum contrast of 22% is observed for the dark line and the bright atoms are still laser-cooled and maintain the ion cloud dynamical stability by sympathetic cooling of the dark atoms (see Fig. 1,**c**). This cooling is efficient enough to keep the ion cloud in a liquid phase all over the frequency scan, which offers the great advantage of keeping the number of trapped ions constant during the whole recording. The splitting of the dark line into several pairs of lines is due to the local magnetic field which lifts the degeneracy of the Zeeman sub-states. We identify each transition according to its Zeeman shift on the THz transition frequency $\delta_Z(m_{THz}) = m_{THz}\mu_B B$ (see Supplemental Material for the relation between the Zeeman shift and the electronic level properties). The stability of each line center frequency is limited by the long term fluctuations of the local magnetic field measured to 0.4 mG (pk-pk). It contributes an uncertainty proportional to m_{THz} and of the order of 1 kHz. The short term fluctuations of the total local magnetic field are measured to 6 mG (pk-pk) and are responsible for a m_{THz}-dependent broadening of the order of 20 kHz (pk-pk).

In a first step, to prove that these dark lines result from the 3-photon process and are referenced to the THz transition, we focus on the dark line defined by $m_{THz} = -13/5$ because of its high contrast. The R-laser frequency ω_R is scanned for different values of ω_C in an interval of 16 MHz, while ω_B is kept constant. The frequency step is 1 kHz and signal is accumulated for 150 ms at each step. Each scan is reproduced 4 times and averaged. Each observed line profile is fitted to a Lorentzien profile and the center of the line ω_R^c is pointed with an uncertainty of the order of 1 kHz (1 σ) conditioned by the frequency step and the signal to noise ratio. The frequency combination $\Delta_{RCB} = \omega_R^c + \omega_C - \omega_B$ is expected to give access to the magnetic transition frequency, once the experimental shifts removed, the Zeeman shift being the largest one identified. Exploiting several multiline spectra as the one of Fig. 1(**e**), the Zeeman shift $\delta_Z(-13/5)$ is evaluated with an uncertainty of ± 6 kHz dominating the total uncertainty of the THz frequency. As shown on Fig 2, the Zeeman corrected transition frequencies are shifted from the $3D_{3/2}$ to $3D_{5/2}$ transition frequency f_{DD} of reference [19], by values which evolve between +5 and -15 (± 6) kHz. These shifts are plotted against the detuning $\Delta_R^Z = \omega_R^c - \omega_{P_{1/2}D_{3/2}} + \delta_R^Z(-13/5)$ with $\omega_{P_{1/2}D_{3/2}}$ the frequency of the atomic transition measured in [28] and $\delta_R^Z(-13/5)$ the Zeeman shift on the R-transition. This plot shows a correlation between the shifts and the detunings that cannot be explained by any drifts in the experimental set-up, neither by the coupling on the quadrupole transition δ_C.

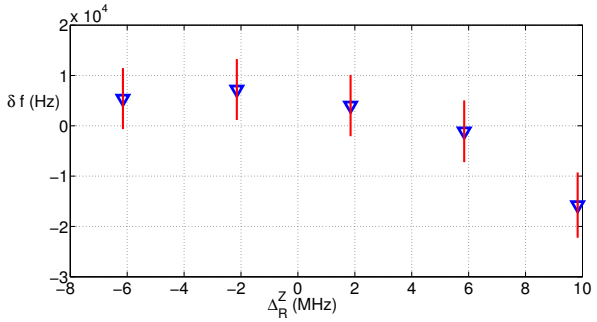

FIG. 2. Frequency shift δf on the 1.8 THz transition [19], for the $m_{THz} = -13/5$ dark line observed for 5 different sets of $\{\omega_C, \omega_B\}$, versus the one photon detuning Δ_R^Z that fits the three photon resonance condition. The Zeeman effect is substracted from the shift ($\delta f = \Delta_{RCB} - \delta_Z(-13/5) - f_{DD}$) and added to the measured one-photon detuning for the Zeeman shifted R-transition (Eq.1). Fixed values : $P_B =$ 10 mW, $P_R = 2$ mW, $P_C = 8$ mW, $\Delta_B = -24.94$ MHz (errorbar= ± 1 std).

When the 729 nm laser power is increased, the frequency shift of the $m_{THz} = -13/5$ line reaches a stationary value for a laser power P_C larger than 10 mW. This is consistent with the model developed to explain the three-photon CPT by a laser mediated two-photon CPT [16] and can be interpreted as a minimum coupling strength requirement to reach an effective CPT. We further use the analogy with two-photon CPT to track laser-induced shifts. In this scheme, the strongest laser coupling is the one driving the R-transition. The observed dependence of the THz-frequency shifts with the power P_R for different Zeeman transitions shows that several power-induced effects add up to build a global frequency shift. Furthermore, the extrapolations of the shifts to zero laser power do not cross the same value, ranging 5 to 15 kHz and speak also for non R-laser power induced effects, like the

one identified above. There are several causes for laser induced shifts in two-photon CPT [29] and some are known to depend on the one-photon detuning [30] and on the ratio of the effective intensity responsible for the laser coupling on the two legs of the Λ-scheme [31, 32]. In the case of a three-photon CPT, the corresponding one-photon detuning is Δ_R and the corresponding intensity ratio R_I is $(\Omega_R\Delta_C/(\Omega_B\Omega_C))^2$ with $\Omega_R, \Omega_B, \Omega_C$ the Rabi frequencies on each transition [16]. On Figure 3, we plot these measured frequency shifts against the modified ratio $R_I \times |\Delta_R^Z|$ for each transition m_{THz}. To that purpose, we take into account the differences in Ω_R, Ω_C, Δ_R^Z and Δ_C^Z for the transition between different Zeeman sub-levels (Ω_B is the same for all the shown transitions-see Supplemental Material). These plots group the shifts measured

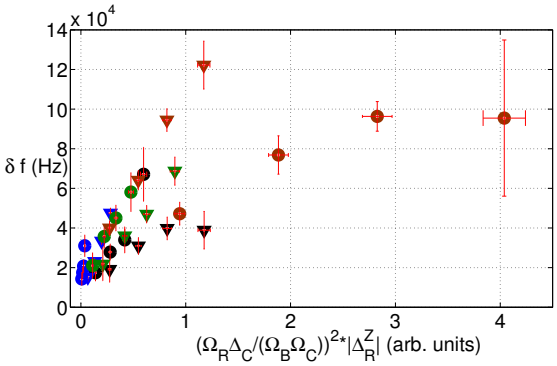

FIG. 3. Frequency shift of the THz-transition identified by their Zeeman shift m_{THz} vs $(\Omega_R\Delta_C/(\Omega_B\Omega_C))^2 \times |\Delta_R^Z|$ measured for a laser power $P_R = 0.7; 1.4; 2.1; 3$ mW. The other laser powers are P_B=19 mW and P_C=10.4 mW. The detuning of the R-laser without any Zeeman effect is -3.8 MHz and the ones of the C-laser is -26.3 MHz. The color codes is brown for $m_{THz} = \pm 3/5$, green for $m_{THz} = \pm 11/5$, blue for $m_{THz} = \pm 13/5$ and black for $m_{THz} = \pm 21/5$, triangles for $-|m_{THz}|$ and circle for $+|m_{THz}|$.

for 8 different transitions on 4 different lines, meaning that the foreseen dependence matches only partially the experimental observations. The interplay of the three laser coupling parameters to explain the measured shift deserves a more detailed study to identify the condition for control and/or cancellation of these shift. One solution to reduce the impact of the power-induced shift may be the implementation of pulsed Ramsey-type protocoles which prove to be very efficient to reduce power-induced effect on two-photon CPT-clocks [33–35].

To quantify the metrological performance of the 3-photon CPT dark line as a THz reference, let's assume these shifts are under control and focus on the line-width, the absolute signal level as well as the contrast of the dark line. We recall that within the present experimental set-up, each line is broadened by the Doppler effect (estimated to a minimum of 20 kHz FWHM) and by a fluctuating Zeeman effect (estimated to $8.4 \times m_{THz}$ kHz pk-pk). Furthermore, in the range of our experimental parameters, the observed power-induced broadening is only due to the coupling on the R-transition. The narrowest observed dark lines (line-width of 45 kHz for $P_R = 0.7$ mW) are the one with the smallest coupling on the R-transition, identified by $|m_{THz}| = 11/5$ and $13/5$ (see table 1 in Supplemental Material). The maximum dark line contrast, reaching 25%, is observed for the lines $|m_{THz}| = 13/5$ and $21/5$ and they are the ones with the largest coupling on the C-transition. These two independent conditions point $|m_{THz}| = 13/5$ as the transition of the best contrast/broadening compromise in the context of our present experimental set-up.

Coming back to the results of Fig. 2 where the $m_{THz} = -13/5$ dark line is observed for different frequencies of the C-laser, we can plot the line-width and contrast for these five different sets of $\{\omega_C, \omega_B\}$ (see Fig. 4). The

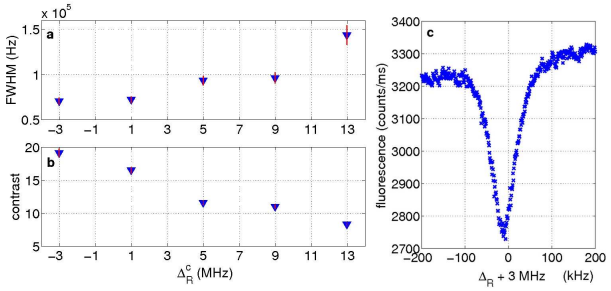

FIG. 4. FWHM (a) and contrast (b) of the $m_{THz} = -13/5$ dark line observed for 5 different sets of $\{\omega_C, \omega_B\}$, vs Δ_R^c, same experiments as for Fig. 1. (c) : line profile of the dark line showing the largest contrast and the smallest line-width of these 5 observations. The background induced by stray light is 520 ± 25 counts/ms.

data show a dependence of the line-width and contrast with the effective value of the detuning Δ_R for which the CPT occurs while all the laser powers are kept constant. We think this effect depends on the relative position of the dark line in the broader fluorescence spectra profiles of the trapped ions, due to a competition with the strong transitions involved in laser cooling. Further inquiries are required to identify the best condition to reach the contrast/line-width optimum but these curves open very positive perspectives as we find in the same detuning range the smallest shifts, the largest contrast and the smallest line-width.

Considering that the Doppler broadening can be cancelled by obeying the phase matching condition $\vec{k}_B - \vec{k}_R - \vec{k}_C = 0$ [11], or eventually by a Lamb-Dicke effect on the THz-wavelength scale [36], the signal over noise ratio could be increased with a larger number of ions building the dark line. When varying the number of trapped ions

from 60 to 400 ions, with all other parameters fixed, we observe no variation of the THz-frequency shift, neither of the dark line width. As the magnetic field fluctuations can be actively reduced by a factor 50 and the sensitivity to these fluctuations can also be reduced by using the transitions $m_{THz} = \pm 1/5$ if other laser polarisation and propagation directions are permitted by the set-up, a line-width in the kHz range, or lower, together with a large contrast seems very accessible. It would enable to access a resolution in the 10^{-9} range, which is the state of the art in the THz precision spectroscopy [36, 37]. In a system without any experimentally induced decoherence, on can show that sub-kHz line-widths can be observed [11]. Nevertheless, with a 25% contrast and an average fluorescence signal of 4000 counts/ms which is the typical value for the fluorescence of one thousand trapped ions in the optimum condition for a narrow dark line, the signal to noise ratio at 1 ms reaches 16. Even with a kHz line-width, such a large signal to noise ratio allows the resolution to be increased to the 10^{-11} range by averaging data over seconds.

This new 3-photon CPT has a large potential for high-resolution spectroscopy. Very similar to 2-photon CPT, the interrogation protocole depends on numerous parameters that have to be further explored. The originality of our approach allows not only to access an insufficiently explored and very promising spectral domain but also to implement a Doppler-free technique which opens the route to its implementation on a large variety of atomic systems.

This experiment has been financially supported by the Labex FIRST-TF (ANR-10-LABX-48-01), the A*MIDEX project (ANR-11-IDEX-0001-02), EquipEx Refimeve+ (ANR-11-EQPX-0039) all funded by the Investissements d'Avenir French Government program, managed by the French National Research Agency (ANR). Fundings from CNES (contract 151084) and Région PACA are acknowledged. MC acknowledges FIRST-TF for funding and stimulating scientific environnement, CyC acknowledges financial support from CNES and Région Provence-Alpes-Cote d'Azur.

[1] Jerome Faist, Federico Capasso, Deborah L. Sivco, Carlo Sirtori, Albert L. Hutchinson, and Alfred Y. Cho. Quantum cascade laser. *science*, 264, 1994.

[2] Yu Yao, Anthony J. Hoffman, and Claire F. Gmachl. Mid-infrared quantum cascade lasers. *Nature Photonics*, 6:432 EP –, 06 2012.

[3] Stefano Barbieri, Pierre Gellie, Giorgio Santarelli, Lu Ding, Wilfried Maineult, Carlo Sirtori, Raffaele Colombelli, Harvey Beere, and David Ritchie. Phase-locking of a 2.7-thz quantum cascade laser to a mode-locked erbium-doped fibre laser. *Nature Photonics*, 4, 2010.

[4] Marco Ravaro, Vishal Jagtap, Christophe Manquest, Pierre Gellie, Giorgio Santarelli, Carlo Sirtori, Suraj P. Khanna, Edmund H. Linfield, and Stefano Barbieri. Spectral properties of thz quantum-cascade lasers: Frequency noise, phase-locking and absolute frequency measurement. *Journal of Infrared, Millimeter, and Terahertz Waves*, 34(5):342–356, Jun 2013.

[5] Bérengère Argence, Bruno Chanteau, Olivier Lopez, Daniele Nicolodi, Michel Abgrall, Christian Chardonnet, Christophe Daussy, Benoit Darquié, Yann Le Coq, and Anne Amy-Klein. Quantum cascade laser frequency stabilization at the sub-Hz level. *Nature Photonics*, 9, 2015.

[6] T. Yasui. 15 - terahertz frequency metrology based on frequency comb techniques. In Daryoosh Saeedkia, editor, *Handbook of Terahertz Technology for Imaging, Sensing and Communications*, Woodhead Publishing Series in Electronic and Optical Materials, pages 436 – 463. Woodhead Publishing, 2013.

[7] T. Udem, J. Reichert, R. Holzwarth, and T. W. Hänsch. Accurate measurement of large optical frequency differences with a mode-locked laser. *Optics Letters*, 24:881, 1999.

[8] Takeshi Yasui, Yasuhiro Kabetani, Eisuke Saneyoshi, Shuko Yokoyama, and Tsutomu Araki. Terahertz frequency comb by multifrequency-heterodyning photoconductive detection for high-accuracy, high-resolution terahertz spectroscopy. *Applied Physics Letters*, 88(24):241104, 2006.

[9] David T. Leisawitz, William C. Danchi, Michael J. DiPirro, Lee D. Feinberg, Daniel Y. Gezari, Mike Hagopian, William D. Langer, John C. Mather, Samuel Harvey Moseley, Michael Shao, Robert F. Silverberg, Johannes G. Staguhn, Mark R. Swain, Harold W. Yorke, and Xiaolei Zhang. Scientific motivation and technology requirements for the spirit and specs far-infrared/submillimeter space interferometers. *Proc.SPIE*, 4013:4013 – 4013 – 11, 2000.

[10] L. Consolino and P. Bartalini, S.and De Natale. Terahertz frequency metrology for spectroscopic applications: a review. *Journal of Infrared, Millimeter, and Terahertz Waves*, 38(11):1289–1315, Nov 2017.

[11] C. Champenois, G. Hagel, M. Houssin, M. Knoop, C. Zumsteg, and F. Vedel. Terahertz frequency standard based on three-photon coherent population trapping. *Phys. Rev. Lett.*, 99(1):013001, 2007.

[12] J. Vanier. Atomic clocks based on coherent population trapping: a review. *Applied Physics B*, 81(4):421–442, Aug 2005.

[13] Shigeo Nagano, Motohiro Kumagai, Hiroyuki Ito, Masatoshi Kajita, and Yuko Hanado. Phase-coherent transfer and retrieval of terahertz frequency standard over 20 km optical fiber with 4×10^{-18} accuracy. *Applied Physics Express*, 10(1):012502, 2017.

[14] Michael Ramm, Thaned Pruttivarasin, Mark Kokish, Ishan Talukdar, and Hartmut Häffner. Precision measurement method for branching fractions of excited $P_{1/2}$ states applied to $^{40}Ca^{+}$. *Phys. Rev. Lett.*, 111:023004, Jul 2013.

[15] M. Knoop, C. Champenois, G. Hagel, M. Houssin, C. Lisowski, M. Vedel, and F. Vedel. Metastable lifetimes from electron-shelving measurements with ion clouds and single ions. *Eur. Phys. J. D*, 29:163, 2004.

[16] Caroline Champenois, Giovanna Morigi, and Jurgen Eschner. Quantum coherence and population trapping

in three-photon processes. *Phys. Rev. A*, 74(5):053404, 2006.

[17] E. Arimondo. Coherent population trapping in laser spectroscopy. volume 35 of *Progress in Optics*, page 257. Elsevier, 1996.

[18] Rekishu Yamazaki, Hideyuki Sawamura, Kenji Toyoda, and Shinji Urabe. Stimulated raman spectroscopy and the determination of the D-fine-structure level separation in $^{40}Ca^{+}$. *Phys. Rev. A*, 77:012508, Jan 2008.

[19] C. Solaro, S. Meyer, K. Fisher, M. V. DePalatis, and M. Drewsen. Direct frequency-comb-driven raman transitions in the terahertz range. *Phys. Rev. Lett.*, 120:253601, Jun 2018.

[20] C. Champenois, J. Pedregosa-Gutierrez, M. Marciante, D. Guyomarc'h, M. Houssin, and M. Knoop. A double ion trap for large coulomb crystals. *AIP Conference Proceedings*, 1521(1):210–219, 2013.

[21] M. R. Kamsap, J. Pedregosa-Gutierrez, C. Champenois, D. Guyomarc'h, M. Houssin, and M. Knoop. Fast and efficient transport of large ion clouds. *Phys. Rev. A*, 92:043416, Oct 2015.

[22] J. Pedregosa, C.Champenois, M. Houssin, and M.Knoop. Anharmonic contributions in real rf linear quadrupole traps. *Int. J. Mass Spec.*, 290:100, 2010.

[23] M. Drewsen, C. Brodersen, L. Hornekær, J. S. Hangst, and J. P. Schifffer. Large ion crystals in a linear Paul trap. *Phys. Rev. Lett.*, 81(14):2878–2881, 1998.

[24] Leaf Turner. Collective effects on equilibria of trapped charged plasmas. *Phys. Fluids*, 30:3196, 1987.

[25] L. Hornekær and M. Drewsen. Formation process of large ion coulomb crystals in linear Paul traps. *Phys. Rev. A*, 66(1):013412, Jul 2002.

[26] R. Wynands and A. Nagel. Precision spectroscopy with coherent dark states. *Applied Physics B*, 68(1):1–25, Jan 1999.

[27] Mathieu Collombon, Gaëtan Hagel, Cyril Chatou, Didier Guyomarc'h, Didier Ferrand, Marie Houssin, Caroline Champenois, and Martina Knoop. Phase transfer between three visible lasers for coherent population trapping. *Opt. Lett.*, 44(4):859–862, Feb 2019.

[28] Florian Gebert, Yong Wan, Fabian Wolf, Christopher N. Angstmann, Julian C. Berengut, and Piet O. Schmidt. Precision isotope shift measurements in calcium ions using quantum logic detection schemes. *Phys. Rev. Lett.*, 115:053003, Jul 2015.

[29] Thomas Zanon-Willette, Emeric de Clercq, and Ennio Arimondo. Ultrahigh-resolution spectroscopy with atomic or molecular dark resonances: Exact steady-state line shapes and asymptotic profiles in the adiabatic pulsed regime. *Phys. Rev. A*, 84:062502, Dec 2011.

[30] P. R. Hemmer, M. S. Shahriar, V. D. Natoli, and S. Ezekiel. Ac stark shifts in a two-zone raman interaction. *J. Opt. Soc. Am. B*, 6(8):1519–1528, Aug 1989.

[31] Peter Yun, Fran çois Tricot, Claudio Eligio Calosso, Salvatore Micalizio, Bruno François, Rodolphe Boudot, Stéphane Guérandel, and Emeric de Clercq. High-performance coherent population trapping clock with polarization modulation. *Phys. Rev. Applied*, 7:014018, Jan 2017.

[32] J. W. Pollock, V. I. Yudin, M. Shuker, M. Yu. Basalaev, A. V. Taichenachev, X. Liu, J. Kitching, and E. A. Donley. ac stark shifts of dark resonances probed with ramsey spectroscopy. *Phys. Rev. A*, 98:053424, Nov 2018.

[33] F.-X. Esnault, E. Blanshan, E. N. Ivanov, R. E. Scholten, J. Kitching, and E. A. Donley. Cold-atom double-Λ coherent population trapping clock. *Phys. Rev. A*, 88:042120, Oct 2013.

[34] E. Blanshan, S. M. Rochester, E. A. Donley, and J. Kitching. Light shifts in a pulsed cold-atom coherent-population-trapping clock. *Phys. Rev. A*, 91:041401, Apr 2015.

[35] Moustafa Abdel Hafiz, Grégoire Coget, Michael Petersen, Cyrus Rocher, Stéphane Guérandel, Thomas Zanon-Willette, Emeric de Clercq, and Rodolphe Boudot. Toward a high-stability coherent population trapping cs vapor-cell atomic clock using autobalanced ramsey spectroscopy. *Phys. Rev. Applied*, 9:064002, Jun 2018.

[36] S. Alighanbari, M. G. Hansen, V. I. Korobov, and S. Schiller. Rotational spectroscopy of cold and trapped molecular ions in the lamb–dicke regime. *Nature Physics*, 14(6):555–559, 2018.

[37] Guoqing Hu, Tatsuya Mizuguchi, Xin Zhao, Takeo Minamikawa, Takahiko Mizuno, Yuli Yang, Cui Li, Ming Bai, Zheng Zheng, and Takeshi Yasui. Measurement of absolute frequency of continuous-wave terahertz radiation in real time using a free-running, dual-wavelength mode-locked, erbium-doped fibre laser. *Science Report*, 7, 2017.